

See discussions, stats, and author profiles for this publication at: <https://www.researchgate.net/publication/251554563>

Combustion of an Illinois No. 6 coal char simulated using an atomistic char representation and the ReaxFF reactive force field

ARTICLE *in* COMBUSTION AND FLAME · MARCH 2012

Impact Factor: 3.08 · DOI: 10.1016/j.combustflame.2011.10.022

CITATIONS

40

READS

73

5 AUTHORS, INCLUDING:



Amar M. Kamat

Pennsylvania State University

3 PUBLICATIONS 67 CITATIONS

[SEE PROFILE](#)



Adri C.T. van Duin

Pennsylvania State University

361 PUBLICATIONS 8,207 CITATIONS

[SEE PROFILE](#)



Jonathan Paul Mathews

Pennsylvania State University

104 PUBLICATIONS 941 CITATIONS

[SEE PROFILE](#)



Combustion of an Illinois No. 6 coal char simulated using an atomistic char representation and the ReaxFF reactive force field

Fidel Castro-Marcano ^a, Amar M. Kamat ^b, Michael F. Russo Jr. ^b, Adri C.T. van Duin ^b, Jonathan P. Mathews ^{a,*}

^aJohn and Willie Leone Family Department of Energy and Mineral Engineering, The EMS Energy Institute, The Pennsylvania State University, University Park, PA 16802, USA

^bDepartment of Mechanical and Nuclear Engineering, The Pennsylvania State University, University Park, PA 16802, USA

ARTICLE INFO

Article history:

Received 2 August 2011

Received in revised form 20 October 2011

Accepted 24 October 2011

Available online xxxx

Keywords:

Char structure

Structural modeling

Fuel-lean combustion

Fuel-rich combustion

ABSTRACT

Coal or biomass chars are complex carbonaceous materials that are important energy sources for electricity production. Reactive molecular dynamics simulations are a useful tool to examine the chemical reactions occurring in complex processes, providing that a realistic structural representation and an applicable reactive force field can be utilized. Combustion of coal (or biomass) char is one such area where additional insight would be helpful for utilization enhancements and pollution control. In this investigation a devolatilized Illinois No. 6 coal char atomistic representation was generated, using Fringe3D and additional Perl scripts, coupled with the ReaxFF reactive force field for hydrocarbon combustion. Fringe3D facilitates the char structure generation process by producing a distribution of aromatic structures based on HRTEM lattice fringe image analyses. Perl scripts were used for incorporating heteroatoms and aliphatic components to aid elimination of investigator bias, and facilitate a more rapid construction process. The char structure was constrained by a combination of elemental and NMR literature data. Chemical and physical parameters were found to be broadly consistent with the experimental data. The ReaxFF force field for hydrocarbon combustion was used to perform simulations to examine the structural transformations and chemical processes associated with char combustion. In this initial work, very high temperatures (3000–4000 K) were selected for ReaxFF simulation under stoichiometric, fuel lean and rich combustion conditions. These elevated temperatures were chosen to observe chemical reactions proceed to completion within a computationally practical simulation time. Analyses indicated that char oxidation process was primarily initialized by either thermal degradation of char structure to form small fragments, that were subsequently oxidized, or by hydrogen abstraction reactions by oxygen molecules and O and OH radicals. A more rapid oxidation and combustion of the polycyclic aromatic structures occurred at fuel lean (oxygen rich) conditions compared with fuel rich combustion. Char transitions included 6-membered ring conversion into 5- and 7-membered rings that further decomposed or reacted with mostly O and OH radicals. This work further demonstrates the utility of ReaxFF force field integration with representative char structural models to investigate physical and chemical transformations of char structure during combustion at high-temperature conditions.

© 2011 The Combustion Institute. Published by Elsevier Inc. All rights reserved.

1. Introduction

Coals are complex carbonaceous structures used as primary combustion fuel sources in electric power generation. Coal supplies 27% of global primary energy needs and currently provides 41% of electricity generation worldwide [1]. The development of realistic atomistic representations can contribute to a better understanding of the structure and behavior relationship of coal char during conversion processes and greatly improve the design strategies for the

effective utilization of coal char in gasification and combustion systems. Coal undergoes rapid loss of moisture and volatiles at high temperatures often followed by thermoplastic transformations resulting in a complex char structure that is dependent on the precursor properties, time-temperature history, and gas pressure employed [2–7]. Devolatilized coal-derived chars are typically highly aromatic (aromaticities of >0.90) and exhibit various degrees of turbostratic crystalline order (stacking, layer size and interlayer spacing), pore size distributions, surface areas, and atomic H/C ratio's [5,8–10]. These variations affect char reactivity [3,11]. The structure of char has a significant impact on subsequent conversion processes such as char gasification and combustion [12–15]. During combustion, the char structure undergoes several

* Corresponding author.

E-mail addresses: fzc108@psu.edu (F. Castro-Marcano), acv13@psu.edu (A.C.T. van Duin), jmatthews@psu.edu (J.P. Mathews).

structural transformations and complex chemical reactions [16]. Coal combustion generally involves devolatilization to form char particles with the release of volatiles followed by their combustion (homogeneous gas-phase reaction) and char particle oxidation and combustion (heterogeneous surface reaction with oxygen) [16–18]. The oxidizing agent must diffuse to the char particle reaction sites, sometimes through the developing ash layer. The reaction products then diffuse away from the char particle [16–18]. For coal char combustion by oxygen, the ratio of the primary combustion products, CO/CO₂, generally increases with increasing temperatures [18].

Despite extensive research, understanding the fundamental reaction mechanisms and chemical events involved in coal char combustion is desirable. Reactive molecular dynamics (MD) simulations can provide insight at the atomistic scale for such reactive events, provided that a representative char structure can be generated and coupled with an appropriately developed reactive force field.

Structural modeling of char structure is challenging, time-consuming, and requires considerable expertise due to the distribution of structural features that often influence the behavior of chars during kinetic controlled conversion reactions. Inorganic species influence char reactivity and have been explored using both experimental [19] and small-scale high-level molecular modeling approaches [20–22], but are not included in this initial work. Various coal-derived char molecular models have been generated by modifying existing coal molecular structures to reflect structural transformations of coal to char during devolatilization [23–25]. Alternative approaches using reverse Monte Carlo (RMC) methods have also been used to construct coal-char structural models for exploring char microstructure and dissolution in steel [26]. The RMC approach uses a reconstruction technique that systematically rearranges the position of atoms via Monte Carlo-type moves until close agreement with experimental small angle X-ray diffraction data is achieved. This approach has been utilized for porous carbon structure [26–29]. However, carbon modeling via RMC methods requires advanced computing capabilities and is more appropriate for highly organized structures. Recently, a more rapid alternative structure generation approach (Fringe3D) has enabled inclusion of nanostructural features and their distributions in model space for carbon materials such as coals, chars and soots directly from HRTEM lattice fringe images [30,31]. With this approach and additional Perl scripts, very large continuum representations (>60,000 atoms) better capturing structural diversity can be generated rapidly with improved accuracy, greater length scale, and minimal computational cost [31]. Fringe3D coupled with Perl scripts for structural manipulation and evaluation was recently utilized in the generation of a large-scale coal molecular model in an effort to move toward capturing the continuum of an Illinois No. 6 coal [32]. Here Fringe3D was used for microstructural modeling of crystalline regions of an Illinois No. 6 coal char atomistic representation from HRTEM micrographs to demonstrate the model construction approach in capturing turbostratic crystalline parameters such as stacking height, layer size and interlayer spacing. These structural nuances influence kinetically controlled char reactivity. For the first time a coal-char molecular model was coupled with a reactive force field to perform reactive MD simulations of char combustion. Coupling ReaxFF combustion with coal-char structural models will greatly improve our design strategies for coal and biomass combustion applications, and air pollution control [14,33–35].

Development of reactive force fields (RFFs) enable description of the formation, transition, and complete dissociation of chemical bonds during reactive MD simulations with accuracy close to quantum mechanics (QM) but with significantly reduced computational expenses. Since RFF parameters are often derived from QM data and

can simulate reaction pathways without any preconditioning, reactive MD simulations via RFF approaches is a powerful tool for examining complex reactive systems. Furthermore, recently developed parallel ReaxFF schemes [36] enable simulations at scale for highly complex structures. Several RFF schemes have been developed and applied to a wide range of materials and applications [37–42]. In particular, the ReaxFF reactive force field has been utilized in several studies to investigate initial reaction mechanisms and kinetics associated with hydrocarbon, fuels, soot and coal thermolysis processes including pyrolysis [43–46], combustion [47–50], and oxidation [42,48,49,51]. While reactive force fields are less computationally expensive than QM methods, they still require considerable computing resources to provide a detailed description of chemical reaction for large and highly complex systems such as coal chars simulated in this work. With current computational resources, the time scale of reactive simulations is many orders of magnitude shorter than that used in the experiments. Thus, reactive simulations are often performed at temperature ranges extending beyond normal experimental/industrial conditions to enable chemical reactions to occur within a practical computational time. With advances in computing power and software tools, reactive MD simulations over longer time scales and lower temperatures will be reachable. Nevertheless, ReaxFF method coupled with a more realistic coal char representation is a useful initial computational approach for examining complex char oxidation and combustion reactions.

Chenoweth et al. [42] expanded the ReaxFF reactive force field training set to include additional transition states and chemical reactivity of systems relevant to hydrocarbon oxidation and optimized the force field parameters against a QM-based training set. They demonstrated that ReaxFF simulations on various hydrocarbon/O₂ systems reproduced the correct reactivity trend, following the trend in the C–H bond strength in these hydrocarbons. Analysis of trajectories from simulations also showed that pathways predicted by ReaxFF were in agreement with QM results and available experimental data.

Recently, the ReaxFF reactive force field for hydrocarbon combustion was extended to incorporate sulfur-containing hydrocarbons. ReaxFF parameters were determined through optimization against an extensive training set obtained from QM data describing reaction barriers and energies associated with C/H/O/S compounds. The newly trained ReaxFF was found to correctly simulate pyrolysis and combustion dynamics of coal molecules and hydrocarbons containing sulfur functionalities [52]. Castro-Marcano et al. [53] utilized the newly trained ReaxFF to perform pyrolysis simulations on a large-scale molecular model for Illinois No. 6 coal constructed based on experimental data [54] to investigate the effect of sulfur content and local sulfur chemistry on the pyrolyzed coal structure. These and previous reactive MD simulations [46] demonstrated the feasibility of ReaxFF integration with coal molecular models and the capability of the newly implemented ReaxFF to provide accurate descriptions of initial reactive events associated with coal pyrolysis. Here ReaxFF was used to perform combustion simulations on a molecular representation for a devolatilized Illinois No. 6 coal char to examine the structural evolution of char structure and chemical processes related to combustion under high-temperature conditions. This work provides an improved char construction methodology and further demonstrates ReaxFF combustion with coal char structural models.

2. Computational methods

2.1. Char model generation

The Fringe3D [31] construction approach was applied to generate atomistic representations for the polyaromatic sheets of the

char structure based on HRTEM lattice fringe data and constrained by elemental analysis [9,55]. HRTEM has been used for characterization of coal and char structures producing structural results in agreement with several analytical techniques but with the advantage of capturing the distribution of nanostructural features [10,11,55–58]. HRTEM lattice fringe image analysis provides structural information on the degree of turbostratic crystalline order (length and stacking of parallel polycyclic aromatic layers as indicated by the fringes) in carbons [55,56]. The methodology of application of HRTEM technique and image processing approach utilized to extract lattice fringes are discussed elsewhere [57,59].

Image Processing Toolkit [60] coupled with Adobe Photoshop was used to perform image analysis for a HRTEM lattice fringe micrograph of an Illinois No. 6 coal char sample heat-treated at 800 °C for 5 min (heating rate: 30 °C/min) [55]. The extracted fringe lengths along with a specific catenation growth were used by Fringe3D to place fringes in 3D molecular modeling space with the assumption that the fringes are all in the same z-plane. Molecules can be placed at the correct Cartesian location, rotated and pitched to duplicate HRTEM lattice fringe images stacking, or assembled in a flat arrangement to better show the distribution of structural features. Currently, fringe curvature was not considered and all fringes were duplicated as flat molecules. Assumption for the shape of the polycyclic aromatic sheets (catenation style) creating the fringes allowed conversion of fringe length to the number of rings in the molecule [31]. Here circular catenation was considered for building the polycyclic aromatic layers of char model. Figure 1 shows an example catenation molecule with polycyclic aromatic structures of C₂₄ to C₅₄. Addition of 6-membered rings around the central rings enables larger polycyclic aromatic structures of varying carbon numbers to be generated. Thus, a circular ring-by-ring growth can occur to accommodate the fringe length distribution. With this construction approach, polycyclic aromatic structures with zigzag and armchair sites, which have been found to exhibit different reactivities [61,62], are created and thus enhancing model structural (and reactive) diversity. In this manner, polycyclic aromatic sheets with a range of sizes and shapes were generated in accordance with known coal char chemistry.

Five-membered rings were manually incorporated into the polycyclic aromatic layers to contain heteroatoms by randomly removing a protonated carbon from an edge 6-membered ring and then creating the respective carbon–carbon covalent bond for ring closure and geometry optimization. Non-hexagonal rings (containing only carbon atoms), recognized as important structural features of the char structure [63], have been incorporated into RMC-derived char models on amounts of up to 15% [26–28,64]. Here, about 6% of non-hexagonal aromatic rings (5- and 7-membered rings) were distributed randomly throughout the largest sheets. Incorporation of aliphatic structures was conducted in the form of hydroaromatic units and cross-linking bridges between layers until agreement with desired aromaticity value of >0.90 was achieved.

Elemental analysis data for an Illinois No. 6 coal char prepared at similar conditions to the sample used for HRTEM analyses, 800 °C for 5 min with heating rate of 50 °C/min [9], was utilized to further constrain the char model. Unfortunately, information regarding the type and distribution of heteroatoms in the coal char sample was not available [9]. Hence, oxygen functionalities were restricted primarily to phenolic, carbonyl and furanic structures, whereas nitrogen and sulfur atoms were placed in pyrrolic and quaternary, and thiophenic type structures respectively, which is consistent with known coal char chemistry [65–67]. Heteroatoms were incorporated into polycyclic aromatic layers by selecting specific atoms using a random-number generator and then replacing them by appropriate functionalities. Specifically, aromatic hydrogens were randomly replaced by phenolics and carbonyls, whereas aromatic carbons in 5- and 6-membered rings were randomly substituted for heteroatoms to generate furanic, thiophenic and pyrrolic structures, and quaternary nitrogen, respectively. A trimming procedure similar to that utilized in previous works [32,68] was performed by randomly removing outer aromatic rings from polycyclic aromatic layers until agreement with the experimental atomic H/C and O/C ratios [9] was achieved. Incorporation of heteroatom and aliphatic components with limited cross-linking was conducted using Perl scripts to remove researcher structural bias, improve accuracy of the structure generated and facilitate a more rapid model construction process.

The resulting polycyclic aromatic layers were geometry-optimized and then assembled into 3D molecular model using the Theodoros and Suter method [69], which randomly distributed the constructed layers into a periodic simulation cell based on a minimum energy criterion. The 3D molecular model was constructed with an initial low bulk density of 0.5 g/cm³ to prevent overlapping of polycyclic aromatic layers in the final structure. The density of the system was then adjusted using successive compression and annealing cycles [70]. Energy minimizations and compression and annealing cycles were performed within Materials Studio package [71] using the consistent-valence force field [72]. Since the structural information employed for char model construction was derived from data sets at different time–temperature histories, the resulting structural model corresponds to a generic representation for the crystalline portion of a devolatilized Illinois No. 6 coal char.

2.2. Model evaluation

Perl scripts developed for coal structural modeling [32,68] were modified and utilized to facilitate model construction and evaluation of chemical and physical structural parameters. These Perl scripts calculate the type and distribution of atoms and functional groups present in the char model. Chemical parameters included elemental composition, carbon aromaticity and molecular weight distribution; whereas physical parameters comprised simulated helium density, pair correlation function, pore size distribution, and turbostratic crystalline dimensions. The simulated helium

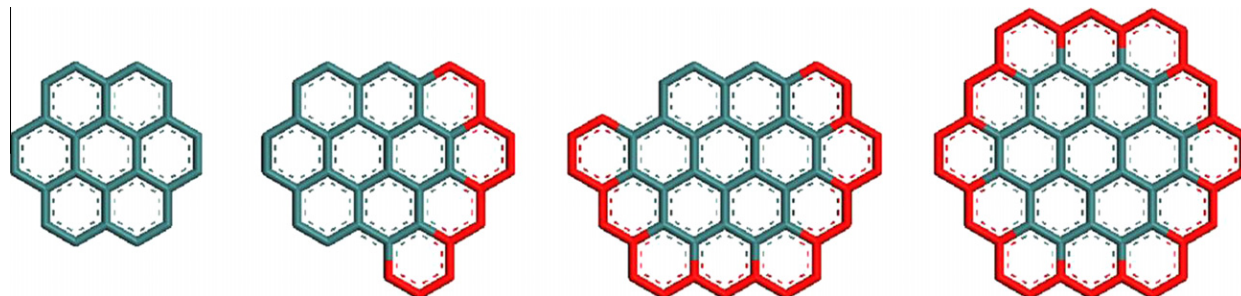


Fig. 1. Examples of polycyclic aromatic structures of C₂₄-to-C₅₄ transitions generated from a circular catenation molecule.

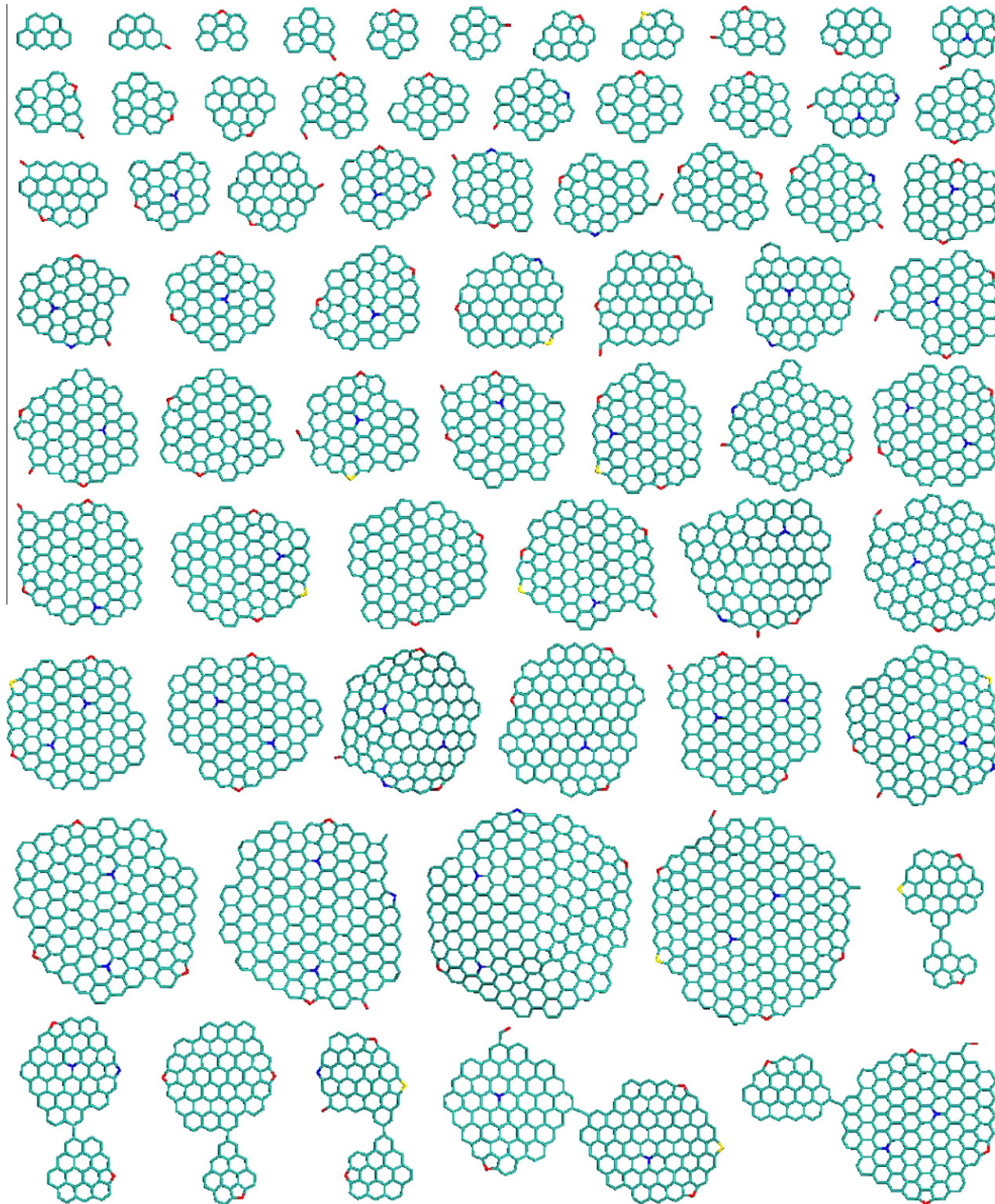


Fig. 2. Polyaromatic hydrocarbon molecules generated by Fringe3D coupled with Perl scripts based on HRTEM lattice fringe data, showing (top) non-cross-linked and (bottom) cross-linked polyaromatic layers. Carbon atoms are colored green, hydrogen atoms are white, oxygen atoms are red, nitrogen atoms are blue, and sulfur atoms are yellow. (For interpretation of the references to color in this figure legend, the reader is referred to the web version of this article.)

density was calculated from the molar mass and the volume of the char structure following an approach similar to that presented by Gelb and Gubbins [73]. The simulation cell is divided into a fine grid and a probe particle is placed at every grid point to determine if an overlap occurs with the char structure. The grid points are sorted as occupied and unoccupied. The sum of the volume of all occupied grid points defines the volume of the char structure, while that of all unoccupied grid points corresponds to the pore volume. The pore size distribution was determined from the plot

of $-dV_{\text{pore}}(r)/dr$ versus r , where $V_{\text{pore}}(r)$ is the fraction of pore volume that can be enclosed by a probe particle of radius r . It is important to note that the porosity of the char model was sampled at the micropore length scale (i.e., not including the macro or mesoporosity) due to the scale of the atomistic representation. Macro- and mesoporosity are expected to influence coal char reactivity and mass transfer during oxidation and combustion, since the oxidizing agents must diffuse to the char reaction sites and the reaction products must diffuse away from the char particle [74].

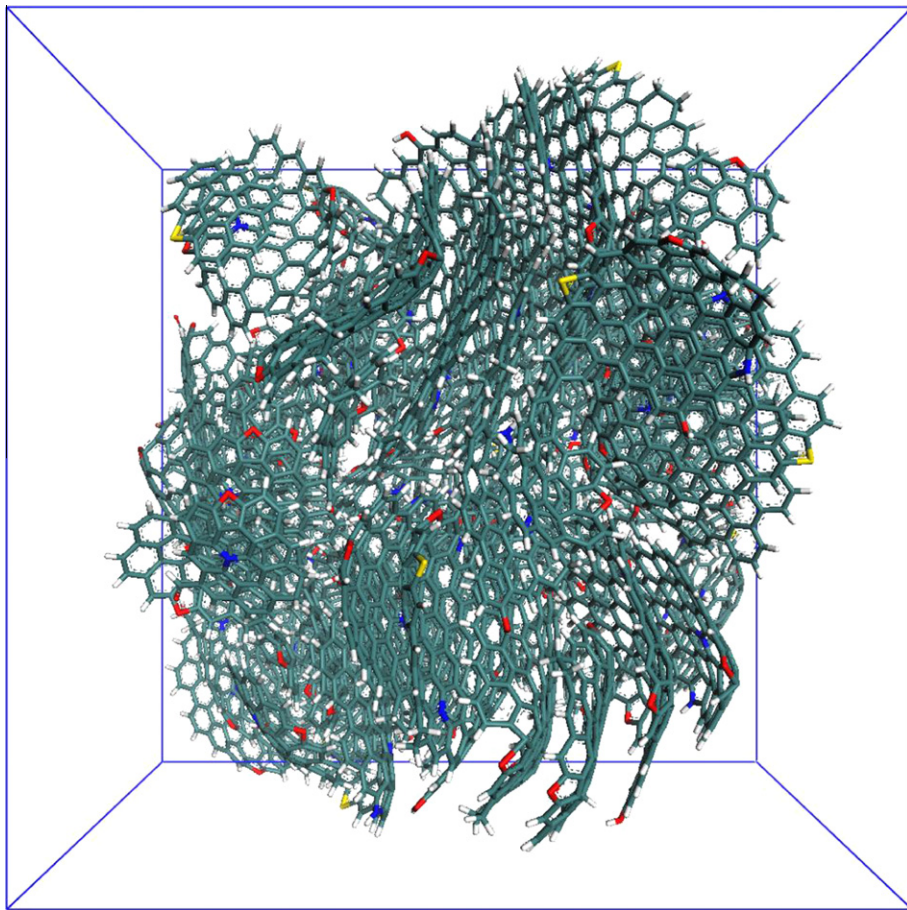


Fig. 3. Atomistic representation for the crystalline regions of a devolatilized Illinois No. 6 coal char composed of 7458 atoms ($C_{5743}H_{1511}O_{131}N_{61}S_{12}$) within 66 polyaromatic layers. The length of the periodic cubic box is 43 Å.

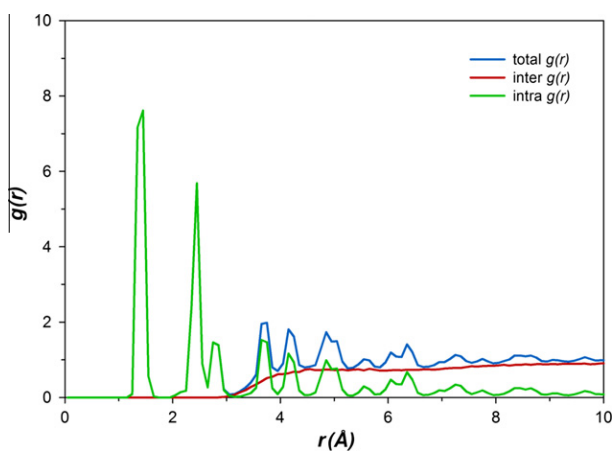


Fig. 4. Pair correlation function for carbon atoms within the Illinois char model. The total $g(r)$ function is the sum of intermolecular (inter $g(r)$) and intramolecular (intra $g(r)$) contributions.

Unfortunately, the small-scale of the char model (~5 nm) compared to coal char particles sizes (typically in the micrometer range) represents a challenging problem for the structural modeler. A simple calculation shows that approximately $15,000 \times 15,000 \times 15,000$ models (3.4×10^{12} models) would be required to fill the same volume as a single 65 µm particle (assuming a cubic particle for ease of calculation). Thus, macro and mesopores were not included and mass transport within the simulated char structure cannot be realistically considered.

The pair correlation function, $g(r)$, provides the probability of finding an atom at a given distance r from another atom. The $g(r)$ function can be calculated from $g(r) = 4\pi r^2 [\rho(r) - \rho_0]$, where $\rho(r)$ and ρ_0 are the pair density at distance r and the average number density, respectively. Stacks of polyaromatic sheets with an inclination angle within $\pm 10^\circ$ were considered for calculation of turbostratic crystalline parameters. These stacks were manually classified according to the number of layers per stack or stacking number. Interlayer spacing and layer length were manually measured as the perpendicular distance between layers forming a stack, and the projected length of the layers, respectively, using molecular modeling software.

2.3. ReaxFF reactive force field

ReaxFF [38] is a reactive force field based on the covalent bonding formalism of Tersoff [75] and Brenner [76] in which the bond strength and bond length adjust appropriately in response to changes in the local chemical environment, resulting in accurate descriptions of bond cleavage and bond formation during chemical reactions. The total potential energy of the system is decomposed into several contributions as:

$$E_{\text{system}} = E_{\text{bond}} + E_{\text{over}} + E_{\text{under}} + E_{\text{val}} + E_{\text{pen}} + E_{\text{tors}} + E_{\text{conj}} + E_{\text{vdWaals}} + E_{\text{Coulomb}} \quad (1)$$

where E_{bond} corresponds to the bond energy, E_{over} and E_{under} represent atom under- and over-coordination, respectively. Other terms, including E_{val} , E_{pen} , E_{tors} , E_{conj} , E_{vdWaals} , and E_{Coulomb} are the valence angle term, penalty energy term, torsion angle energy, conjugation

effects to molecular energy, non-bonded van der Waals interactions and Coulombic interactions, respectively. The ReaxFF potential determines the system connectivity based on bond orders calculated from interatomic distances that are updated every iteration, enabling dissociation and formation of chemical bonds during reactive MD simulations. Morse and Coulomb potentials were utilized for modeling the non-bonded interactions (van der Waals and Coulomb), which were calculated between all atom pairs and were shielded at short range. A geometry-dependent charge calculation scheme [77] was used to account for polarization effects. ReaxFF parameters were derived from quantum chemical calculations on bond dissociation and reactions of small molecules as well as heat of formation, transition state energy and geometry data for several simple hydrocarbons [38]. A more detailed description of the ReaxFF potential functions can be found in the work by van Duin et al. [38].

2.4. Molecular dynamics simulation details

For the oxidation/combustion simulations, three periodic cubic boxes of 140, 165 and 195 Å box length were built containing the char structure composed of 7458 atoms along with 3500, 7000, and 14,000 O₂ molecules, respectively. These periodic systems (char + oxygen) with different oxygen concentrations were generated to analyze the effect of combustion environment on the final products distribution. The equivalence ratio (ϕ) for these systems was 0.5, 1.0, and 2.0, which correspond to fuel lean, stoichiometric, and fuel rich combustion. The equivalence ratio being defined as the fuel/oxygen ratio normalized with respect to the stoichiometric fuel/oxygen ratio. These systems were energy-optimized using the conjugate gradient method and equilibrated via low-temperature (100 K) ReaxFF simulations (time step of 0.25 fs) to prevent chemical reactions from occurring during equilibration. The temperature was controlled using the Berendsen thermostat [78] with a 0.1 ps damping constant. The temperature of these equilibrated systems was ramped up to 4000 K at a rate of ~24 K/ps with the system states (i.e., atomic positions, velocities and accelerations)

saved at 3000, 3500 and 4000 K. Thereafter, constant temperature MD simulations were conducted for each periodic system for 250 ps at temperatures of 3000, 3500 and 4000 K. The highly complex char representation generated in this study required reactive simulations at elevated temperatures to enable complete combustion of the char structure within 250 ps. Although fuel combustion processes often occurs within a few seconds at flame temperatures up to 2000 K [14,17], ReaxFF simulations were performed at higher temperatures to allow chemical reactions to occur within a reasonable time scale (in the picoseconds range) with the expectation of exhibiting similar initiation mechanisms to experiments. Previous works have showed that initial reaction mechanisms and kinetics associated with fossil fuel thermolysis processes via high-temperature ReaxFF MD simulations are in qualitative agreement with experimental data [42–50], although the elevated temperature has to be considered in the quantitative analysis of the reaction kinetics. The current simulations were performed within the ReaxFF program as implemented in ADF software [79] using 36 processors on an Intel Xeon X5560 Quad-Core 2.8 GHz at the Lion-XH HPCS of Penn State Research Computing and Cyberinfrastructure [80]. A typical equilibration and production run for the systems investigated in this study took about 4–6 weeks of simulation time (each simulation occupying four processors) followed by multiple weeks of data analysis. With increase in computing resources, longer reactive simulations under conditions of lower temperature will be manageable. Nevertheless, by linking ReaxFF method with representative char models can provide initial insight into complex chemical processes related to coal char combustion. Fortran scripts were developed to create separate trajectories of all polycyclic aromatic sheets in the system to track the structural transformations and chemical reactions during oxidation and combustion.

3. Results and discussion

A total of 72 polycyclic aromatic sheets were generated by Fringe3D coupled with Perl scripts in a highly automated manner, capturing

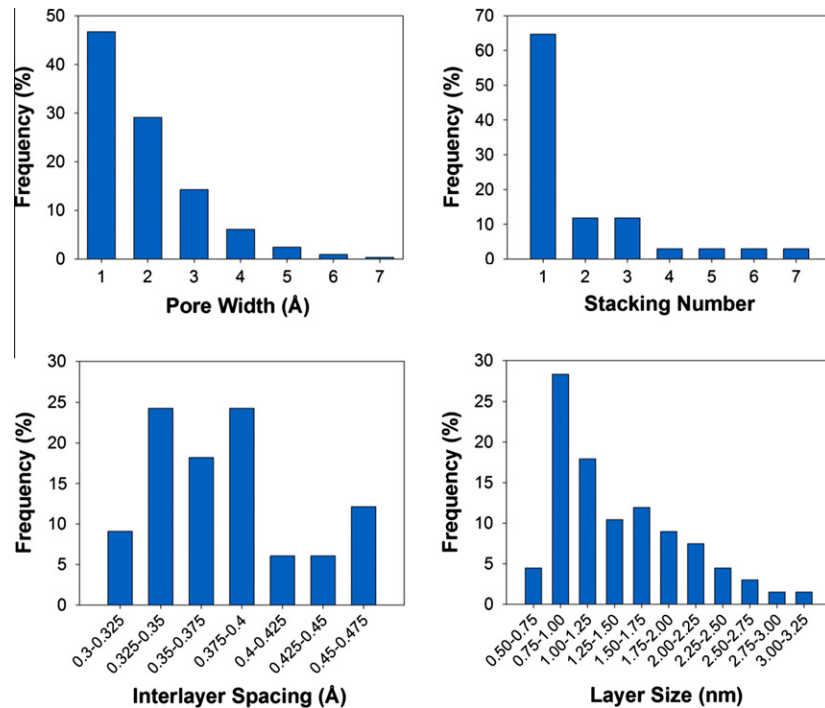


Fig. 5. Distributions of pore size and turbostratic crystalline parameters (stacking number, layer size and interlayer spacing) determined from the Illinois coal char molecular model.

a distribution of structural features in the char structure. The layers were created in order of molecular size and arranged in a flat grid (Fig. 2) to allow visualization of the model construction process. Limited cross-linking produced 66 polycyclic aromatic hydrocarbon structures. Heteroatom and aliphatic components were incorporated by scripting to agree with experimental data. The resultant

polycyclic (and heteroatom containing) structures were geometry-optimized and assembled into a cubic 3D molecular model using Materials Studio Amorphous Cell module [71]. The energy-optimized model for an Illinois No. 6 coal char is shown in Fig. 3. The turbostratic char structure contains 7458 atoms ($C_{5743}H_{1511}O_{131}N_{61}S_{12}$) within 66 polycyclic aromatic molecules and

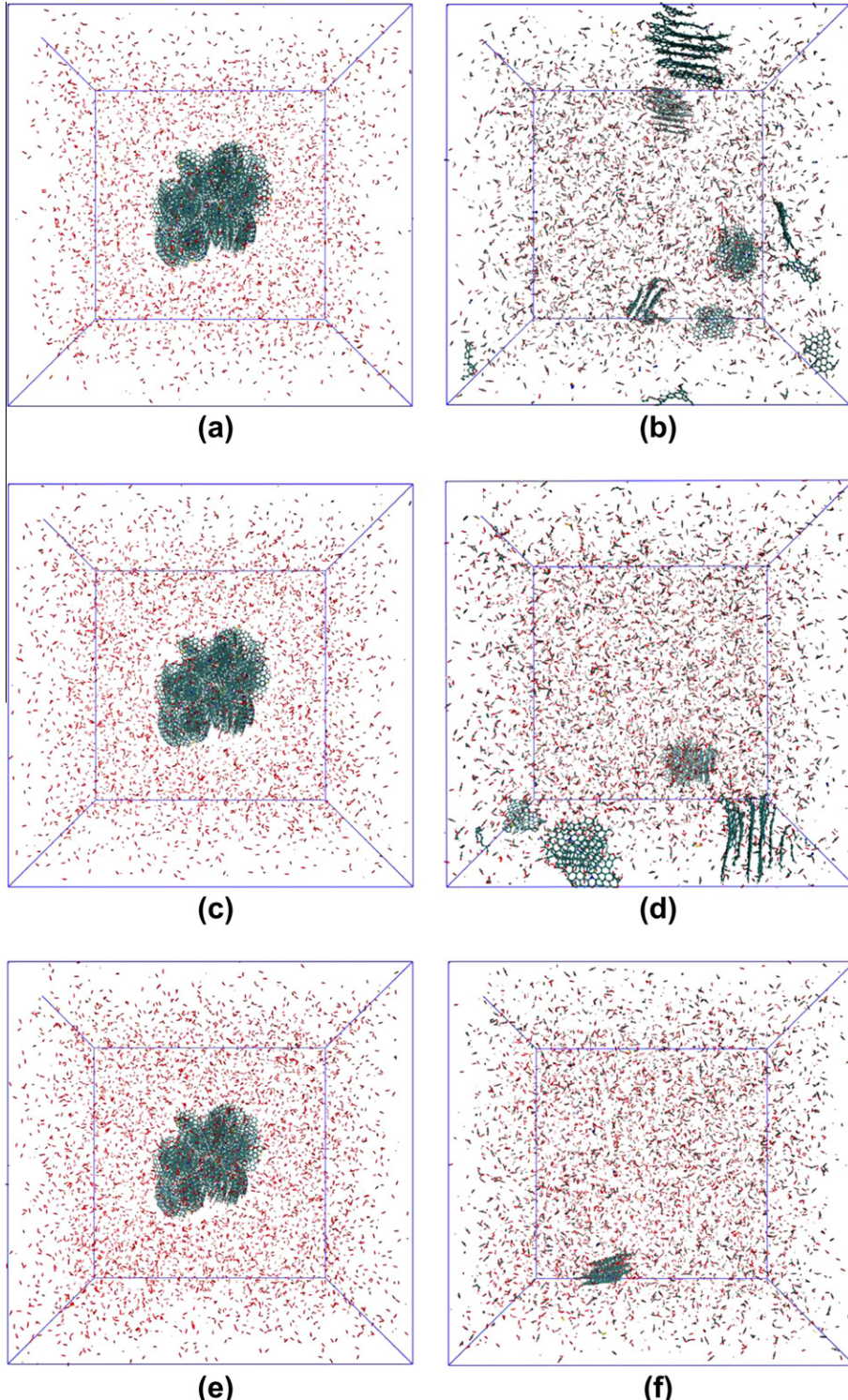


Fig. 6. Snapshots of the equilibrated and final configurations after 250 ps ReaxFF combustion simulation at 3000 K for the fuel rich (a and b), stoichiometric (c and d) and fuel lean (e and f) systems containing the char structure ($C_{5743}H_{1511}O_{131}N_{61}S_{12}$) surrounded by 3500, 7000 and 14,000 O_2 molecules, respectively. Molecular oxygen is represented by sticks and the char structure is represented by the ball-and-stick model with atoms colored as in Fig. 2. (For interpretation of the references to color in this figure legend, the reader is referred to the web version of this article.)

captures a range of structural features including aromatic, aliphatic and heteroatoms components as well as molecule sizes, degree of stacking, and interlayer spacing. The length of the cubic simulation cell was 43 Å.

3.1. Evaluation of chemical and physical structural parameters

The chemical evaluation of the char structure comprised, elemental analysis, aromaticity, and the molecular weight distribution. The elemental composition, normalized to 1000 carbon atoms for the char structural model was $C_{1000}H_{263}O_{23}N_{11}S_2$, in reasonable agreement with the experimental value $C_{1000}H_{252}O_{24}N_{11}S_2$ [9]. The char model aromaticity was 0.96 in accordance with experimental data for devolatilized coal chars [2,5,81]. The char molecular model exhibited a molecular weight distribution ranging from 239 to 3454 Da with a peak at ~250–500 Da, and calculated values for number and weight average molecular weights of 1095 and 1605 Da, respectively.

The physical structure of the char model was characterized in terms of several analytical parameters. The simulated helium

density of the char model was 1.81 g/cm^3 , consistent with the helium density value of $1.7\text{--}1.9 \text{ g/cm}^3$ (dmmf) corresponding to coal chars generated at 800°C [82,83]. The helium density of coal chars is usually expected to be greater than that of parental coals (1.30 g/cm^3 on dmmf for Illinois No. 6 coal [84]) mostly due to an ordering of polyaromatic layers within the coal char matrix along with an increase in aromaticity and release of aliphatic carbons, hydrogen and oxygen during devolatilization. The pair correlation function for carbon atoms within the char model is shown in Fig. 4 with total $g(r)$ being the sum of the intermolecular and intramolecular contributions. The first three peaks in the total $g(r)$ function correspond to separation distances between pair of atoms within the same polyaromatic layer due to the intermolecular contribution to total $g(r)$ is zero. Specifically, the first peak appears at 1.40 \AA due to the presence of sp^3 and sp^2 carbons. This result is consistent with the model aromatic and aliphatic carbon content of 96% and 4% (using 1.39 \AA for aryl C–C bonds and 1.54 \AA for alkyl C–C bonds result in $1.40 \text{ \AA} = 0.96 \times 1.39 \text{ \AA} + 0.04 \times 1.54 \text{ \AA}$). The second and third peaks are at around 2.40 and 2.85 \AA , similar to the second and third peaks for graphite located at 2.46 and

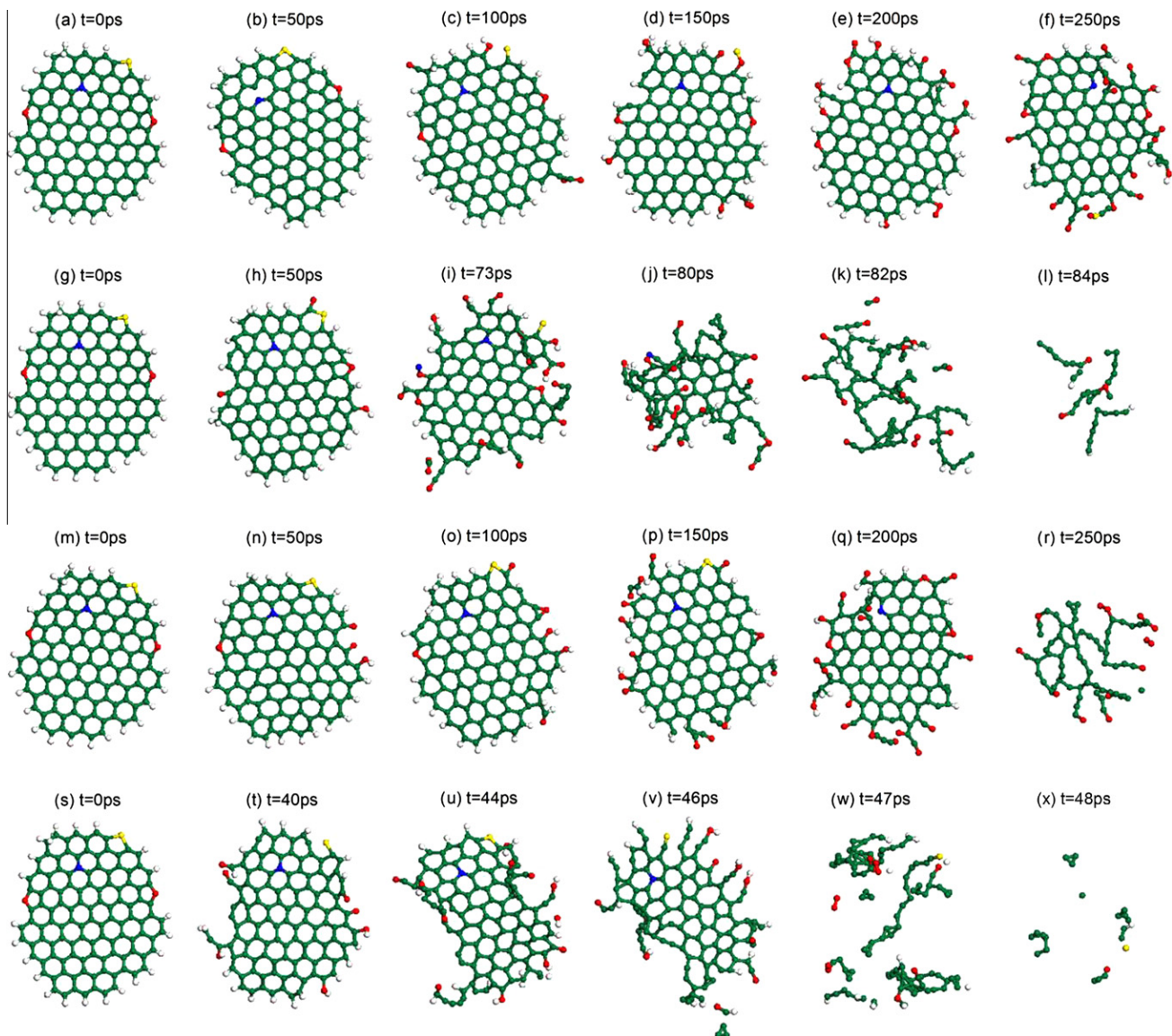


Fig. 7. Snapshots of the combustion process for a representative polyaromatic sheet ($C_{117}H_{24}O_2N_1S_1$) observed during ReaxFF combustion simulations under fuel rich conditions at 3000 K (a–f) and 4000 K (g–l), and in fuel lean at 3000 K (m–r) and 4000 K (s–x). The char sheet is represented by the ball-and-stick model with atoms colored as in Fig. 2. (For interpretation of the references to color in this figure legend, the reader is referred to the web version of this article.)

2.86 Å [29]. Peaks located at $r > 3$ Å are also affected by the stacking and neighboring layers (intramolecular contribution) and thus analysis of the total $g(r)$ function becomes more complex. However, no peaks appeared at ~ 3.4 Å, the layer separation in graphite [29] consistent with shorter polycyclic aromatic layers that are more turbostratic.

Figure 5 shows the distributions of pore size and turbostratic crystalline parameters (stacking number, layer size and interlayer spacing). The pore size distribution showed smooth transitions as the pore width increases with limited fluctuations. The range of pore sizes extends up to about 7 Å with a peak at ~ 1 –2 Å; i.e., the simulated char structure contains a significant portion of micropores with pore widths ranging between 1 and 2 Å. Kulaots et al. [8] examined the role of porosity during char combustion for Argonne coals and reported for an Illinois coal char (prepared at 1000 °C for 1 h in pure He) a pore size distribution ranging from

4 to 60 Å with the char being mostly microporous [8]. Since the simulation cell length employed here was 43 Å, the char model porosity can only be evaluated at the micropore length scale. Nevertheless, increasing the length scale should result in a char model that better accommodates the pore size distribution and molecular diffusion issues. The average interlayer spacing between stacked sheets was ~ 3.8 Å, consistent with XRD data for an Illinois coal char prepared at 1300 °C [10]. The stacking number distribution indicated that the majority of polycyclic aromatic layers are either single or in stacks composed of 2–3 layers with an average value of 2.4, which is in reasonable agreement (given the limited scale) with the values of 3.0 and 3.2 as determined by HRTEM [55] and XRD [10] analyses for Illinois coal char samples. The layer size distribution ranged from 5 to 32.5 Å with an average value of 14 Å, in accordance with reported values of 12 and 14 Å from HRTEM [55] and XRD [10] studies for Illinois coal chars. Therefore, the char

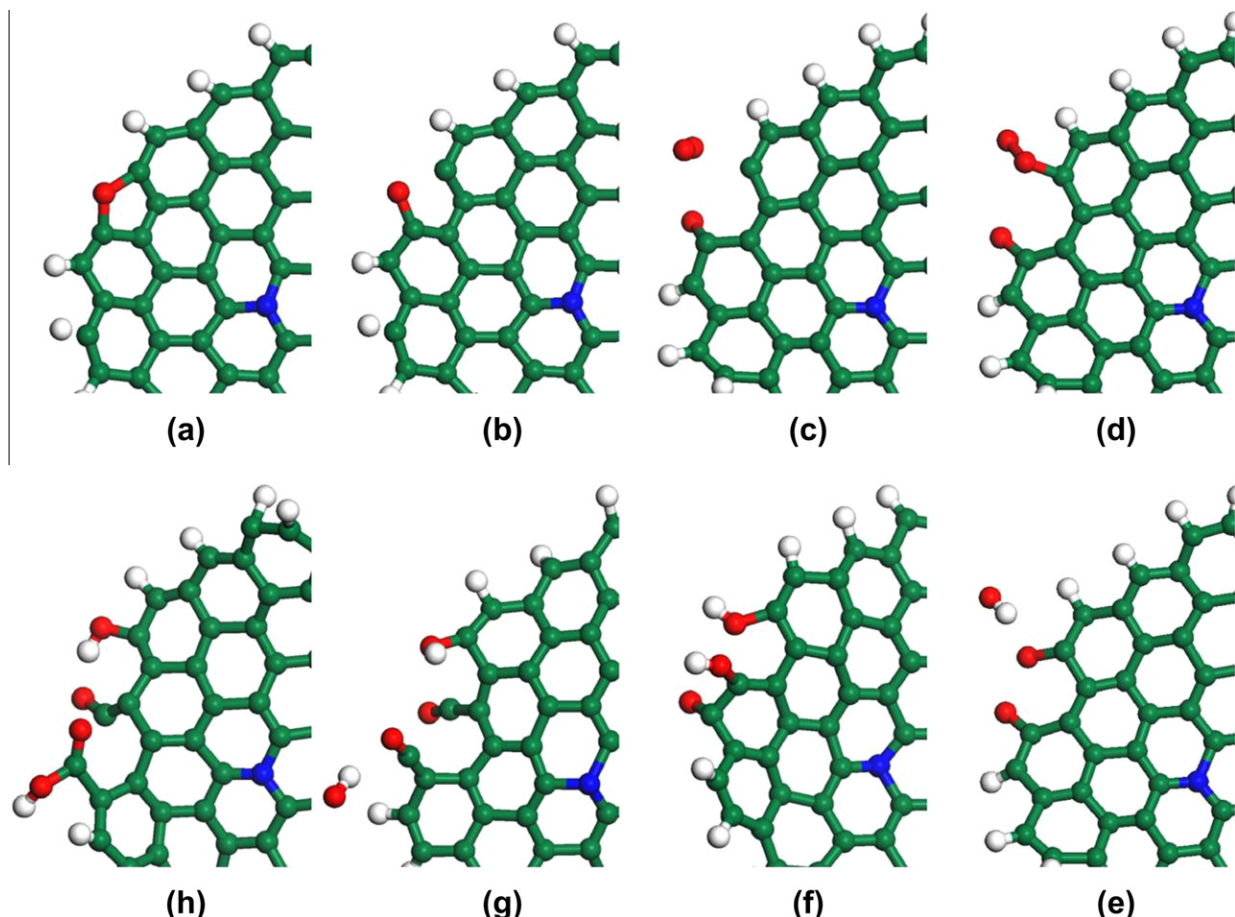


Fig. 8. Example of initial chemical events observed for the oxidation of a polyaromatic sheet ($C_{54}H_{18}O_4N_1$) in the fuel rich system at 3000 K. Dissociation of the C–O bond produced a carbon radical (a and b) that reacted with O_2 molecule to form a carbon–oxygen complex (c and d). Next, release of a hydroxyl radical resulted in formation of two semiquinone groups (e). Subsequent oxidation of the neighboring carbon produced a semiquinone (f), then cleavage of the C–C bond generated a carbon radical that was oxidized to carboxylic group (g and h), followed by decarboxylation leading to CO_2 formation. Atoms are represented using the ball-and-stick model and colored as in Fig. 2. (For interpretation of the references to color in this figure legend, the reader is referred to the web version of this article.)

Table 1

Number of successful oxygen attacks (O_2 molecules, and O and OH radicals) observed after 250 ps ReaxFF combustion simulation.

| Combustion environment | 3000 K | | | | 3500 K | | | | 4000 K | | | |
|------------------------|--------|-------|-----|------------|--------|-------|-----|------------|--------|-------|-----|------------|
| | O | O_2 | OH | Decomposed | O | O_2 | OH | Decomposed | O | O_2 | OH | Decomposed |
| Fuel rich | 798 | 107 | 282 | 7033 | 708 | 98 | 288 | 11,310 | 527 | 75 | 239 | 15,728 |
| Stoichiometric | 916 | 124 | 166 | 8353 | 925 | 106 | 211 | 14,323 | 789 | 117 | 205 | 20,723 |
| Fuel lean | 896 | 132 | 133 | 11,105 | 713 | 127 | 93 | 18,962 | 460 | 97 | 58 | 27,429 |

model generated exhibits the distinct advantage of representing the distribution of nanostructural features observed in HRTEM lattice fringe images and in capturing the turbostratic crystalline dimensions measured by XRD and HRTEM.

3.2. ReaxFF combustion simulations

A series of ReaxFF combustion simulations of the char structure under fuel lean, fuel rich and stoichiometric conditions at high temperatures (3000, 3500 and 4000 K) were performed to evaluate the effects of combustion environment and temperature on the final product distribution. Conducting combustion simulations with different oxygen levels can provide structural information associated with the competitive role of thermal decomposition and direct oxidation by oxygen molecules. However, at these temperatures it is expected that initiation of char oxidation will be a competition between hydrogen abstraction reactions and direct thermolysis. At lower practical temperatures the char oxidation process will be mainly initialized by thermal decomposition and reactions with radicals in the fuel rich system while direct oxidation of the char structure by oxygen molecules and O and OH radicals under fuel lean combustion [42]. Snapshots of the equilibrated and final configurations of the combustion products after 250 ps of ReaxFF simulation at 3000 K for the fuel rich (a and b), stoichiometric (c and d) and fuel lean (e and f) systems are shown

in Fig. 6. Initially, small molecules and fragments were released from the char structure followed by O and OH radical attacks on polyaromatic sheets and molecular fragments in the system (char oxidation) and subsequent combustion of the evolved gases and char structure, in accordance with the fundamental steps of char combustion [16–18]. Snapshots of combustion for a representative polyaromatic sheet ($C_{11}H_{24}O_2N_1S_1$) observed during ReaxFF simulations under fuel rich and lean conditions at 3000 and 4000 K are presented in Fig. 7. The char sheet underwent several changes and structural transformations during combustion. As seen in Fig. 7, the polyaromatic sheet decomposed more rapidly during fuel lean conditions in comparison to fuel rich combustion, and thermal decomposition became more significant with increasing temperature as expected. In general, the radical species (mostly O and OH radicals) were seen to surround and attack the peripheral atoms promoting oxidation/combustion of ring structures.

Analysis of trajectories from ReaxFF simulations showed complex initiation chemistry for the char oxidation process for all combustion conditions studied. In most cases, char oxidation was mostly initialized by either thermal decomposition of char structure to produce small fragments that were subsequently oxidized or hydrogen abstraction reactions by O_2 molecules, and O and OH radicals. An example of initial chemical events observed for the oxidation of a polyaromatic sheet ($C_{54}H_{18}O_4N_1$) in the fuel rich system at 3000 K is shown in Fig. 8. The initial reaction involved

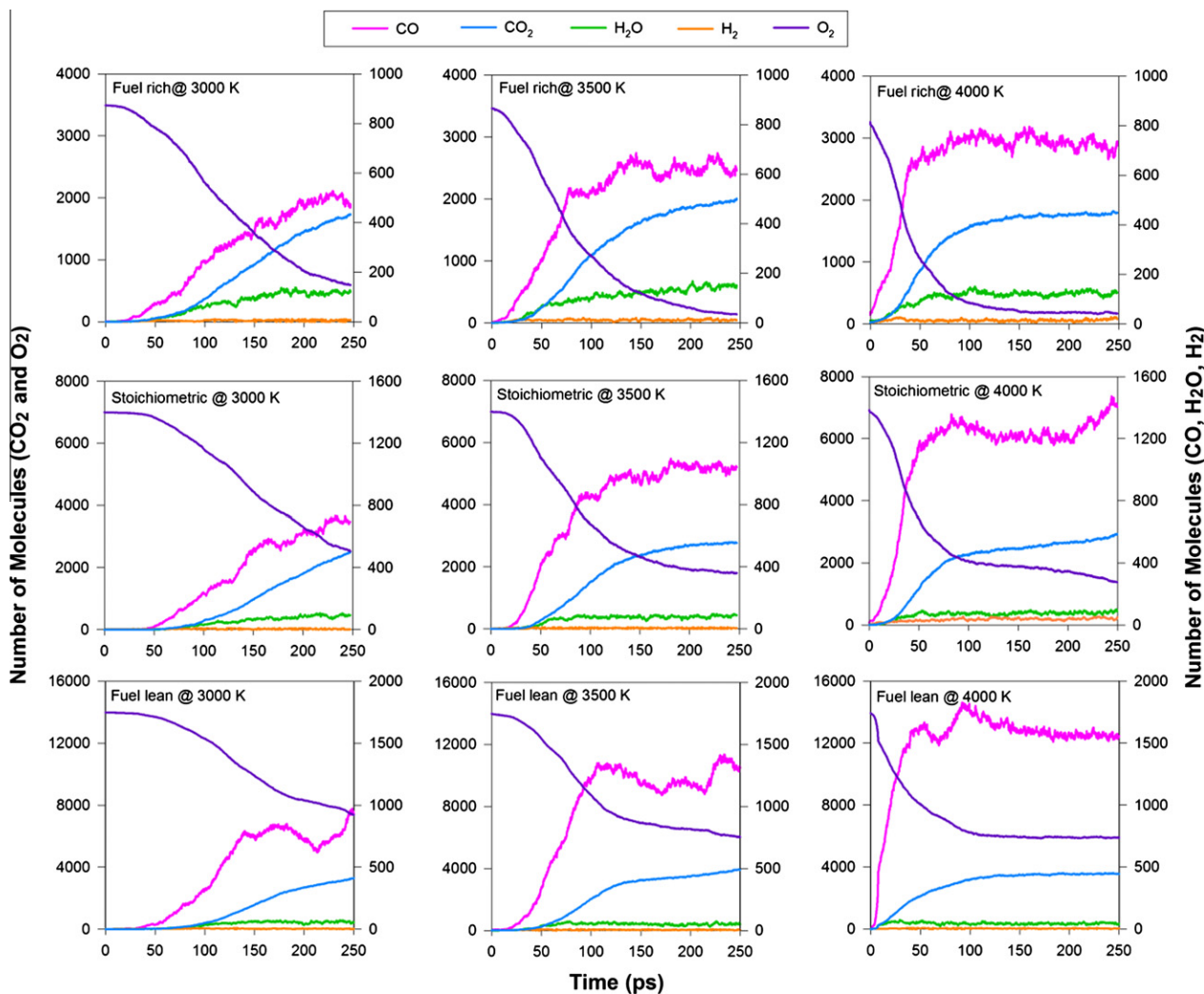


Fig. 9. Distribution of major combustion products obtained from ReaxFF MD simulations of char combustion at temperatures of 3000, 3500 and 4000 K under fuel rich, stoichiometric and fuel lean conditions.

dissociation of the furanic C–O bond to form a carbon radical (Fig. 8a and b) that reacts with molecular oxygen to generate a carbon–oxygen complex (Fig. 8c and d) followed by release of a hydroxyl radical resulting in formation of two semiquinone groups (Fig. 8e). Subsequent oxidation of the neighboring carbon produced a semiquinone (Fig. 8f) and then cleavage of the C–C bond generated a carbon radical that was oxidized to carboxylic group (Fig. 8g and h), followed by decarboxylation leading to CO₂ formation.

Current kinetic modeling methods based on single- or multi-step combustion reaction do not provide an atomistic description of the initial chemical events associated with char oxidation [35,85,86]. Alternative approaches using density functional theory (DFT) calculations on simplistic carbon structures (<50 atoms) have been used to examine carbon–oxygen complexes formed during char gasification [87–89]. These DFT-based studies have shown that initially molecular oxygen is adsorbed on active carbon sites (zigzag and armchair edges) forming peroxide complexes that then transformed into two stable semiquinone groups (by dissociating the O–O bond), which decomposed to release CO by breaking two C–C bonds [87–89]. The advantage of using the ReaxFF force field is that it provides a detailed, dynamical description of complex oxidation reactions for larger and more complex systems over longer time scales.

A Fortran script was created to monitor the major types of oxygen attacks (O₂ molecules, and O and OH radicals), to gain a better understanding of the chemistry during combustion. The number of successful attacks (defined as reactive collisions producing covalent bonds lasting more than 5 ps) observed after 250 ps of simulation is summarized in Table 1. Oxygen attacks on small fragments generated from thermal decomposition of polyaromatic sheets were identified as “decomposed”, whereas attacks on large polyaromatic sheets (>30 atoms) were considered as direct oxidation by O/O₂/OH species. As seen, oxygen attacks on small fragments seem to be more predominant than direct oxidation of large sheets for all combustion environments at the temperature range investigated. In addition, the O and OH radical attacks exhibited the highest rate of success (defined as the ratio of successful attacks and the total number of collisions), which can be attributed to the highly reactive nature of these radical species. Under fuel rich conditions, the radical attack successful rates were higher in comparison to fuel lean because of the lower total number of collisions.

Figure 9 shows the concentration profiles for oxygen and the major combustion products (CO₂, H₂O, CO and H₂) observed during ReaxFF combustion simulations at constant temperature (after the temperature of the system was ramped up) and thus initial amounts of CO₂ and O₂ molecules differ with temperature. In general, the rate of combustion products generation was greater when

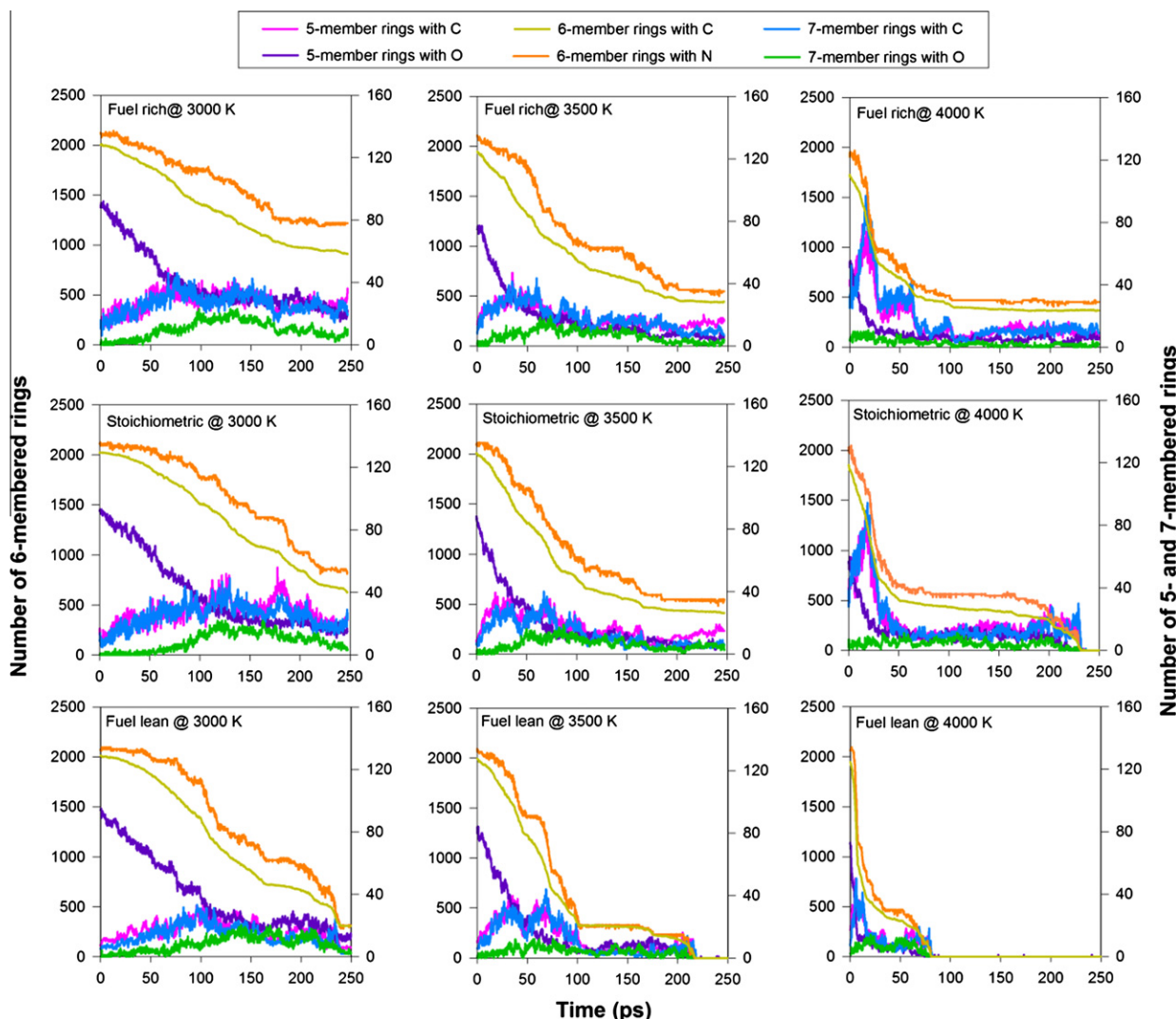


Fig. 10. Time evolution of 5-, 6- and 7-membered rings in the char structure observed in ReaxFF combustion simulations at temperatures of 3000, 3500 and 4000 K under fuel rich, stoichiometric and fuel lean environments.

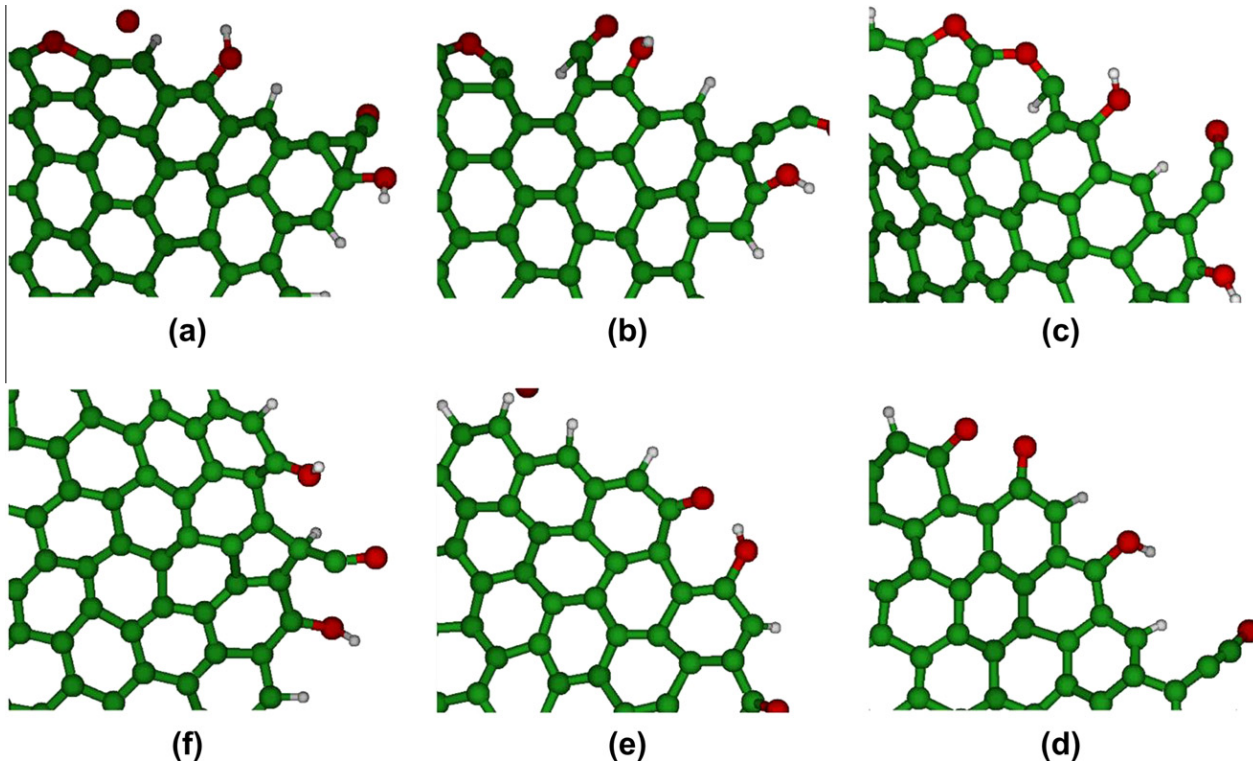


Fig. 11. Example of conversion of 6-membered ring into 5- and 7-membered rings observed during fuel rich combustion at 3000 K. An O radical attack caused 6-membered ring opening and formation of carbon–oxygen complex (a and b). An intermediate heterocyclic 7-membered ring is generated (c), which decomposed to form two semiquinone groups (d). Subsequent intramolecular rearrangement of the C–O bond led to formation of the 5-membered ring (e and f). Atoms are represented using the ball-and-stick model and colored as in Fig. 2. (For interpretation of the references to color in this figure legend, the reader is referred to the web version of this article.)

fuel lean in comparison to fuel rich conditions, in agreement with observations of faster char burning rates for progressively higher O₂ levels [14,35]. At fuel lean combustion ($\phi = 0.5$), CO₂ concentration was higher than that of CO due to an excess of oxygen resulting in a more complete transformation of the char structure to carbon dioxide and water at 250 ps. Under fuel rich conditions ($\phi = 2.0$), there would be incomplete conversion to combustion products and thus CO and H₂ would remain as combustion gases [16]. However, at the end of the simulation, there were around 500–700 molecules of CO in the fuel rich system compared to about 900–1600 CO molecules in the fuel lean system. This is presumably caused by the short time scale (250 ps) used in the ReaxFF simulations. Carbon monoxide oxidation to CO₂ is a relatively slow process among combustion reactions [18]. Thus, it is expected that at longer time scales a portion of CO molecules in the fuel lean system would be oxidized to CO₂.

Figure 9 also shows that the rate of increase of combustion products was almost linear during simulations at the lower temperature (3000 K). This can be contrasted with combustion at 4000 K, where rapid char conversion to combustion products occurred and the concentration of reaction products reached a peak and subsequently leveled off at a relative constant value. In addition, the rate of decrease of O₂ was more rapid and the char structure exhibited shorter initiation reaction times. This is due to char combustion reactions proceed rapidly with increasing temperature [14,35]. Formation of CO was facilitated by high temperatures whereas CO₂ production was favored at the lower temperature studied, as expected because CO is more stable than CO₂ at temperatures higher than 2000 K [16–18]. Small amounts of water and hydrogen were formed during char combustion mostly because of the limited hydrogen content of the char.

A Fortran script was developed to track the evolution of 5-, 6- and 7-membered rings in the char structure, as a function of time,

to gain a better understanding of the chemistry during combustion (Fig. 10). Analysis of the trajectory from the simulations showed that intermediate ring structures (such as 3-, 4- and 8-membered rings) were formed during char combustion but these structures were short lived, hence were not included in the analysis shown in Fig. 10. The char structure was initially composed of 130 5-membered rings (6, 98, 11, and 15 containing C, O, S, and N respectively), 2166 6-membered hydroaromatic rings (135 containing N) and four 7-membered rings containing only C and H atoms. Figure 10 shows the transformations in ring structures corresponding to ReaxFF combustion simulations at constant temperature and thus the initial number of polycyclic ring structures is different for each temperature. As shown, all ring structures decomposed more rapidly in fuel lean (oxygen rich) in comparison to fuel rich environment, at the temperature range used. This can be attributed to the limited oxygen availability in the fuel rich system leading to incomplete combustion of polycyclic aromatic sheets. In fuel lean environment, however, there was sufficient oxygen and time (at this temperature) for complete combustion of the char structure.

At 3000 K, the number of 6-membered rings steadily decreased over the course of the simulations (Fig. 10). The 5-membered rings with O decreased significantly during the earlier stages of the simulation (between 75 and 100 ps) but changed little thereafter. The amount of 7-membered rings and 5-membered rings with C atoms reached peaks before decreasing close to its initial low value. The location of these peaks coincided with a more rapid decomposition of the 6-membered rings suggesting that these ring structures decomposed to form 5- and 7-membered rings, as shown in Fig. 11. Initially, an oxygen radical attacked a 6-membered ring leading to cleavage of the edge C–C bond and formation of the respective carbon–oxygen complex (Fig. 11a and b). Next, the bonded O atom connected to a carbon radical generating a

heterocyclic 7-member ring (Fig. 11c), which afterward decomposed to form two semiquinone groups (Fig. 11d). Subsequent intramolecular rearrangement of the C–O bond formed a 5-membered ring (Fig. 11e and f). Kinetic Monte Carlo simulations of graphene-edge growth in combustion environments showed that high temperatures (>2500 K) lead to kinetic instability of 5-membered rings and thus prevent them from forming in the growing graphene sheet [90].

As the temperature increases (Fig. 10), the number of 6-membered rings and 5-membered rings containing O declined rapidly, and 7-membered rings and 5-membered rings with C atoms reached peaks that were more pronounced. Combustion reactions were accelerated at these high temperatures resulting in ring structures fragmenting. Ultimately, with computational speed gains it is anticipated that this approach could be utilized at boiler combustion temperatures, over long simulation times, with very large-scale char representations. Both large-scale and long time simulations are necessary to capture the char pore size distribution and hence the mass transport issues important in zones III and II. Catalytic influences, important in some chars, could also be included. The work presented here is an initial exploration of the approach while ultimately many orders of magnitude gains in size and time is necessary to simulate particle systems of interest.

4. Conclusions

Fringe3D coupled with Perl scripts were used to generate a structural representation of the crystalline portion of a devolatilized Illinois No. 6 coal char based on HRTEM lattice fringe images and constrained by elemental analysis data. Agreement between model and experimental chemical and physical structural parameters validated the constructed coal char representation. Chemical parameters included elemental composition, carbon aromaticity, and molecular weight distribution; whereas physical parameters comprised simulated helium density, pore size distribution, pair correlation function, and turbostratic crystalline parameters (stacking height, layer size and interlayer spacing).

The ReaxFF reactive force field was applied to perform combustion simulations of the constructed char model under fuel lean, fuel rich and stoichiometric conditions at temperatures of 3000, 3500, and 4000 K to investigate the effects of combustion environment and temperature on the oxidation/combustion process and product distributions. Analysis of trajectories from ReaxFF simulations showed that char oxidation was mainly initialized by either thermal degradation of char structure generating small fragments that were subsequently oxidized, or by hydrogen abstraction reactions by O₂ molecules and O and OH radicals. The ratio of the major combustion products, CO/CO₂, was found to increase with increasing temperature consistent with expectations. Furthermore, ring structures were observed to disintegrate more rapidly in fuel lean conditions in comparison to the fuel rich environment, and 6-membered rings were transformed into 5- and 7-membered rings that subsequently decomposed into smaller fragments. This work demonstrates that coupling the ReaxFF reactive force field with more realistic char molecular models can be a useful simulation approach for examining the complex chemistry associated with structural transformations and chemical reactions involved in char combustion.

Acknowledgments

This project was funded by the Illinois Clean Coal Institute with funds made available through the Office of Coal Development of the Illinois Department of Commerce and Economic Opportunity.

References

- [1] World Coal Association, Annual Energy Report, 2011. <<http://www.worldcoal.org/coal/>>.
- [2] T.H. Fletcher, M.S. Solum, D.M. Grant, R.J. Pugmire, *Energy Fuels* 6 (1992) 643–650.
- [3] J.L. Yu, J.A. Lucas, T.F. Wall, *Prog. Energy Combust. Sci.* 33 (2007) 135–170.
- [4] D. Zeng, T.H. Fletcher, *Energy Fuels* 19 (2005) 1828–1838.
- [5] L.M. Lu, V. Sahajwalla, D. Harris, *Energy Fuels* 14 (2000) 869–876.
- [6] N. Yoshizawa, K. Maruyama, T. Yamashita, A. Akimoto, *Fuel* 85 (2006) 2064–2070.
- [7] K. Kidena, K. Matsumoto, M. Katsuyama, S. Murata, M. Nomura, *Fuel Process. Technol.* 85 (2004) 827–835.
- [8] I. Kulaots, A. Hsu, E.M. Suuberg, *Proc. Combust. Inst.* 31 (2007) 1897–1903.
- [9] K. Matsuoka, T. Akahane, H. Aso, A. Sharma, A. Tomita, *Fuel* 87 (2008) 539–545.
- [10] K.A. Davis, R.H. Hurt, N.Y.C. Yang, T.J. Headley, *Combust. Flame* 100 (1995) 31–40.
- [11] C. Sheng, *Fuel* 86 (2007) 2316–2324.
- [12] H.Y. Cai, A.J. Guell, I.N. Chatzakis, J.Y. Lim, D.R. Dugwell, R. Kandiyoti, *Fuel* 75 (1996) 15–24.
- [13] R.H. Hurt, *Energy Fuels* 7 (1993) 721–733.
- [14] G.S. Liu, S. Niksa, *Prog. Energy Combust. Sci.* 30 (2004) 679–717.
- [15] P.R. Solomon, M.A. Serio, E.M. Suuberg, *Prog. Energy Combust. Sci.* 18 (1992) 133–220.
- [16] R.H. Essenhoff, Fundamentals of coal combustion, in: M.A. Elliott (Ed.), *Chemistry of Coal Utilization*, second Suppl. vol., John Wiley and Sons, New York, 1981, pp. 1153–1312.
- [17] M.L. Hobbs, P.T. Radulovic, L.D. Smoot, *Prog. Energy Combust. Sci.* 19 (1993) 505–586.
- [18] N.M. Laurendeau, *Prog. Energy Combust. Sci.* 4 (1978) 221–270.
- [19] L.R. Radovic, P.L. Walker, R.G. Jenkins, *J. Catal.* 82 (1983) 382–394.
- [20] G. Domazetis, B.D. James, J. Liesegang, *J. Mol. Model.* 14 (2008) 581–597.
- [21] G. Domazetis, B.D. James, J. Liesegang, *Energy Fuels* 22 (2008) 3994–4005.
- [22] G. Domazetis, J. Liesegang, B.D. James, *Fuel Process. Technol.* 86 (2005) 463–486.
- [23] A. Marzec, *Energy Fuels* 11 (1997) 837–842.
- [24] J.M. Jones, M. Pourkashanian, C.D. Rena, A. Williams, *Fuel* 78 (1999) 1737–1744.
- [25] J.P. Mathews, A. van Duin, A. Chaffee, *Fuel Process. Technol.* 92 (2011) 718–728.
- [26] T. Petersen, I. Yarovsky, I. Snook, D.G. McCulloch, G. Opletal, *Carbon* 42 (2004) 2457–2469.
- [27] S.K. Jain, R.J.M. Pellenq, J.P. Pikunic, K.E. Gubbins, *Langmuir* 22 (2006) 9942–9948.
- [28] J. Pikunic, C. Clinard, N. Cohaut, K.E. Gubbins, J.M. Guet, R.J.M. Pellenq, I. Rannou, J.N. Rouzaud, *Langmuir* 19 (2003) 8565–8582.
- [29] T.J. Bandosz, M.J. Biggs, K.E. Gubbins, Y. Hattori, T. Iiyama, K. Kaneko, J. Pikunic, K.T. Thomson, Molecular models of porous carbons, in: L.R. Radovic (Ed.), *Chemistry and Physics of Carbon*, Marcel Dekker, Inc., New York, 2003, pp. 41–228.
- [30] V. Fernandez-Alos, Improved Molecular Model Generation from Soots, Chars, and Coals: HRTEM Lattice Fringes Reproduction with Fringe3D, Ph.D. Thesis, Energy and Mineral Engineering, Pennsylvania State University, 2010.
- [31] V. Fernandez-Alos, J.C.K. Watson, R.L. Vander Wal, J.P. Mathews, *Combust. Flame* 158 (2011) 1807–1813.
- [32] F. Castro-Marcano, V. Lobodin, R. Rodgers, A. McKenna, A. Marshall, J. Mathews, *Fuel*, submitted for publication.
- [33] A.B. Brown, D.C. Dayton, M. Nimlos, J.W. Daily, *Energy Fuels* 15 (2001) 1276–1285.
- [34] S.P. Krumdieck, J.W. Daily, *Combust. Sci. Technol.* 134 (1998) 351–365.
- [35] S. Niksa, G.S. Liu, R.H. Hurt, *Prog. Energy Combust. Sci.* 29 (2003) 425–477.
- [36] A. Nakano, R.K. Kalia, K. Nomura, A. Sharma, P. Vashishta, F. Shimojo, A.C.T. van Duin, W.A. Goddard, R. Biswas, D. Srivastava, *Comput. Mater. Sci.* 38 (2007) 642–652.
- [37] S.J. Stuart, A.B. Tutein, J.A. Harrison, *J. Chem. Phys.* 112 (2000) 6472–6486.
- [38] A.C.T. van Duin, S. Dasgupta, F. Lorant, W.A. Goddard, *J. Phys. Chem. A* 105 (2001) 9396–9409.
- [39] L.P. Huang, J. Kieffer, *J. Chem. Phys.* 118 (2003) 1487–1498.
- [40] A.C.T. van Duin, A. Strachan, S. Stewart, Q.S. Zhang, X. Xu, W.A. Goddard, *J. Phys. Chem. A* 107 (2003) 3803–3811.
- [41] A. Violi, *Combust. Flame* 139 (2004) 279–287.
- [42] K. Chenoweth, A.C.T. van Duin, W.A. Goddard, *J. Phys. Chem. A* 112 (2008) 1040–1053.
- [43] D.E. Jiang, A.C.T. van Duin, W.A. Goddard, S. Dai, *J. Phys. Chem. A* 113 (2009) 6891–6894.
- [44] N. Lummen, *Phys. Chem. Chem. Phys.* 12 (2010) 7883–7893.
- [45] E. Salmon, A.C.T. van Duin, F. Lorant, P.M. Marquaire, W.A. Goddard, *Org. Geochem.* 40 (2009) 416–427.
- [46] E. Salmon, A.C.T. van Duin, F. Lorant, P.M. Marquaire, W.A. Goddard, *Org. Geochem.* 40 (2009) 1195–1209.
- [47] K. Chenoweth, A.C.T. van Duin, S. Dasgupta, W.A. Goddard, *J. Phys. Chem. A* 113 (2009) 1740–1746.
- [48] Q.D. Wang, J.B. Wang, J.Q. Li, N.X. Tan, X.Y. Li, *Combust. Flame* 158 (2011) 217–226.

- [49] A.M. Kamat, A.C.T. van Duin, A. Yakovlev, *J. Phys. Chem. A* 114 (2010) 12561–12572.
- [50] S. Agrawalla, A.C.T. van Duin, *J. Phys. Chem. A* 115 (2011) 960–972.
- [51] A. Bagri, C. Mattevi, M. Acik, Y.J. Chabal, M. Chhowalla, V.B. Shenoy, *Nat. Chem.* 2 (2010) 581–587.
- [52] M.F. Russo, A.M. Kamat, A.C.T. van Duin, F. Castro-Marcano, J.P. Mathews, in preparation.
- [53] F. Castro-Marcano, A.C.T. van Duin, J.P. Mathews, in preparation.
- [54] F. Castro-Marcano, J.P. Mathews, *Energy Fuels* 25 (2011) 845–853.
- [55] A. Sharma, T. Kyotani, A. Tomita, *Fuel* 80 (2001) 1467–1473.
- [56] A. Sharma, T. Kyotani, A. Tomita, *Carbon* 38 (2000) 1977–1984.
- [57] H.S. Shim, R.H. Hurt, N.Y.C. Yang, *Carbon* 38 (2000) 29–45.
- [58] R.H. Hurt, K.A. Davis, N.Y.C. Yang, T.J. Headley, G.D. Mitchell, *Fuel* 74 (1995) 1297–1306.
- [59] A. Sharma, T. Kyotani, A. Tomita, *Fuel* 78 (1999) 1203–1212.
- [60] Image Processing Tool Kit, Reindeer Graphics, Inc., Asheville, NC, 2005.
- [61] L.R. Radovic, *Carbon* 43 (2005) 907–915.
- [62] L.R. Radovic, P.L. Walker, R.G. Jenkins, *Fuel* 62 (1983) 849–856.
- [63] P.F. Harris, Impact of the discovery of fullerenes on carbon science, in: L.R. Radovic (Ed.), *Chemistry and Physics of Carbon*, Marcel Dekker, Inc., New York, 2003, pp. 1–36.
- [64] M. Acharya, M.S. Strano, J.P. Mathews, J.L. Billinge, V. Petkov, S. Subramoney, H.C. Foley, *Philos. Mag. B* 79 (1999) 1499–1518.
- [65] D.W. Van Krevelen, *Coal: Typology, Chemistry, Physics, Constitution*, third ed., Elsevier Science, New York, 1993.
- [66] H.Y. Cai, A.J. Guell, D.R. Dugwell, R. Kandiyoti, *Fuel* 72 (1993) 321–327.
- [67] P.R. Solomon, M.A. Serio, R.M. Carangelo, R. Bassilakis, D. Gravel, M. Baillargeon, F. Baudais, G. Vail, *Energy Fuels* 4 (1990) 319–333.
- [68] D. Van Niekerk, J.P. Mathews, *Fuel* 89 (2010) 73–82.
- [69] D.N. Theodorou, U.W. Suter, *Macromolecules* 18 (1985) 1467–1478.
- [70] D. Hofmann, L. Fritz, J. Ulbrich, C. Schepers, M. Bohning, *Macromol. Theory Simul.* 9 (2000) 293–327.
- [71] Materials Studio Software, Accelrys Inc., San Diego, CA, 2010.
- [72] S. Lifson, A.T. Hagler, P. Dauber, *J. Am. Chem. Soc.* 101 (1979) 5111–5121.
- [73] L.D. Gelb, K.E. Gubbins, *Langmuir* 15 (1999) 305–308.
- [74] P.L. Walker, F. Rusinko, L.G. Austin, *Adv. Catal.* 11 (1959) 133–221.
- [75] J. Tersoff, *Phys. Rev. B* 37 (1988) 6991–7000.
- [76] D.W. Brenner, *Phys. Rev. B* 42 (1990) 9458–9471.
- [77] W.J. Mortier, S.K. Ghosh, S. Shankar, *J. Am. Chem. Soc.* 108 (1986) 4315–4320.
- [78] H.J.C. Berendsen, J.P.M. Postma, W.F. Vangunsteren, A. Dinola, J.R. Haak, *J. Chem. Phys.* 81 (1984) 3684–3690.
- [79] E.J. Baerends, et al., ADF2010, SCM, Theoretical Chemistry, Vrije Universiteit, Amsterdam, The Netherlands. <<http://www.scm.com>>.
- [80] Penn State Research Computing and Cyberinfrastructure. <<http://rcc.its.psu.edu/resources/hpc/>>.
- [81] R.J. Pugmire, M.S. Solum, D.M. Grant, S. Critchfield, T.H. Fletcher, *Fuel* 70 (1991) 414–423.
- [82] R.E. Franklin, *Trans. Faraday Soc.* 45 (1949) 668–682.
- [83] D. Merrick, *Fuel* 62 (1983) 547–552.
- [84] H. Huang, K.Y. Wang, D.M. Bodily, V.J. Hucka, *Energy Fuels* 9 (1995) 20–24.
- [85] R. Barranco, A. Rojas, J. Barraza, E. Lester, *Fuel* 88 (2009) 2335–2339.
- [86] R.H. Hurt, J.M. Calo, *Combust. Flame* 125 (2001) 1138–1149.
- [87] A. Montoya, F. Mondragon, T.N. Truong, *Fuel Process. Technol.* 77 (2002) 125–130.
- [88] R.I. Backreedy, J.M. Jones, M. Pourkashanian, A. Williams, *Proc. Combust. Inst.* 29 (2002) 415–421.
- [89] K. Sendt, B.S. Haynes, *Combust. Flame* 143 (2005) 629–643.
- [90] R. Whitesides, M. Frenklach, *J. Phys. Chem. A* 114 (2010) 689–703.